Modeling top-quark decays in $t\bar{t}t\bar{t}$ production at the LHC

Manal Alsairafi,* Nikolaos Dimitrakopoulos,† and Malgorzata Worek‡
Institute for Theoretical Particle Physics and Cosmology, RWTH Aachen University, D-52056 Aachen, Germany

(Received 21 July 2025; accepted 7 November 2025; published 5 December 2025)

We compare the fixed-order NLO QCD predictions for the $pp \to t\bar{t}t\bar{t} + X$ process in the 4ℓ decay channel with the parton-shower-based results obtained with the Powheg and MC@NLO matching methods. In the first case, NLO QCD corrections are consistently included in both the $t\bar{t}t\bar{t}$ production step and the decays of the four top quarks, preserving all spin correlations. In the second approach, higher-order effects in top-quark decays with approximate spin correlations are simulated in the Pythia parton-shower framework. Additionally, we analyze the impact of including the so-called matrix element corrections in top-quark decays in both parton-shower matched predictions. The comparison is performed at the integrated and differential fiducial cross-section level for the LHC center-of-mass energy of $\sqrt{s} = 13.6$ TeV.

DOI: 10.1103/sm4n-3tcg

I. INTRODUCTION

The $pp \to t\bar{t}t\bar{t}$ process is a fascinating, yet relatively rare process that can be measured at the Large Hadron Collider (LHC). Precisely because it is a rare process, $t\bar{t}t\bar{t}$ production is sensitive to contributions from potential new physics. Many of the new physics scenarios predict effective $t\bar{t}t\bar{t}$ interactions as well as new processes such as $pp \to Y_{\text{new}}Y_{\text{new}}$ and $pp \to t\bar{t}Y_{\text{new}}$, where Y_{new} denotes a new heavy resonance decaying into a $t\bar{t}$ pair, leading to the $t\bar{t}t\bar{t}$ final state. Any significant deviation from the Standard Model (SM) prediction for the $t\bar{t}t\bar{t}$ cross section could hint at these new particles or interactions. Consequently, good theoretical control of the $pp \to t\bar{t}t\bar{t}$ process is a fundamental requirement for the correct interpretation of possible new physics signals that may appear in this channel. In addition, top quarks decay into a bottom quark and a W boson, and the $W^{\pm}$ bosons decay further into leptons or quarks. For the $pp \to t\bar{t}t\bar{t}$ process, this can lead to complicated final states with multiple jets, including b jets, multiple leptons, and missing transverse momentum due to neutrinos that are not detected at the LHC. These rich signatures allow for powerful cross-checks between different theoretical predictions to strengthen confidence in modeling of the SM process, but also bring significant experimental challenges from large backgrounds, especially from $pp \to t\bar{t}W^{\pm}$, $pp \to t\bar{t}W^{\pm} + \text{jets}$, $pp \to t\bar{t}Z/\gamma$, $pp \to t\bar{t}H$ or other processes with multiple leptons and jets.

At the LHC, both ATLAS and CMS measured the $pp \to t\bar{t}t\bar{t}$ cross section at a center-of-mass energy of $\sqrt{s} = 13$ TeV [1,2]. Both measurements are reasonably consistent with the SM prediction, although they are still subject to significant statistical and systematic uncertainties. Over time, as more data is collected, the measurements will become more precise, and analyses will focus on advancing such cross-section measurements, improving background estimation techniques, and looking for possible outliers that might indicate new physics. In addition to the total cross section, differential measurements will be performed and compared to simulated theoretical predictions. These tests would help refine the modeling aspects for this process and highlight potential deviations that might point to new physics effects.

With the high-luminosity upgrade of the LHC on the horizon, even more precise measurements of $t\bar{t}t\bar{t}$ production will become feasible. This must be accompanied by equally precise and accurate theoretical predictions that are under good control. Improved modeling may be key to matching the increased experimental precision. Modeling of the $pp \to t\bar{t}t\bar{t} + X$ process requires a combination of higher-order QCD calculations, careful handling of parton showers, and robust treatment of theoretical uncertainties. The complexity of the $t\bar{t}t\bar{t}$ final state makes accurate simulation particularly important, but also difficult, and should focus on distinguishing these rare events from various background processes.

*Contact author: manal.alsairafi@rwth-aachen.de
†Contact author: ndimitrak@physik.rwth-aachen.de
‡Contact author: worek@physik.rwth-aachen.de

Published by the American Physical Society under the terms of the Creative Commons Attribution 4.0 International license. Further distribution of this work must maintain attribution to the author(s) and the published article's title, journal citation, and DOI. Funded by SCOAP³.

Various theoretical predictions for the $pp \to t\bar{t}t\bar{t}$ process are currently available in the literature, focusing on the precision or accuracy of modeling different final states or both aspects simultaneously. Indeed, in the latter case, they not only take into account higher-order QCD effects, but also the proper treatment of spin correlations in top-quark decays, which is a necessary step to correctly describe many observables, including those sensitive to physics beyond the SM. Therefore, on the one hand, we have NLO QCD predictions for the $pp \to t\bar{t}t\bar{t} + X$ process with stable top quarks [3–5]. Theoretical predictions with the so-called complete NLO corrections are also available [6]. In this case, various leading and subleading contributions, along with their higher-order effects, are consistently taken into account to form the complete NLO result. Recently, the calculation for this process has been carried out at the next-to-leading logarithmic level [7,8]. On the other hand, for realistic studies, one has to consider a 12-particle final state, which consists of four b jets and, depending on the decay channel, additional jets and/or charged leptons with missing transverse momentum. Also, in this case, various theoretical predictions can already be found in the literature. These include the NLO parton shower-matched predictions for the 1ℓ decay channel [9], as well as the fixed-order NLO QCD predictions in the narrow-width approximation for the 4ℓ [10] and 3ℓ decay channels [11]. While these are important theoretical results, they exist as separate predictions for different decay channels. No attempt has yet been made to consistently compare these two approaches for the same decay mode for the $pp \to t\bar{t}t\bar{t} + X$ process. It would be beneficial to compare the fixed-order NLO QCD results with those in which higher-order corrections to top-quark decays are generated by parton showers. Such a comparison could assess to what extent parton showers can approximate higher-order effects in top-quark decays. It would also be able to verify the significance of NLO QCD corrections to angular observables, which are sensitive to top-quark spin correlations as well as to new physics effects. Furthermore, such a comparison could help identify the phase-space regions sensitive to parton-shower effects, describing collinear and soft-collinear emissions with leading logarithmic accuracy.

The purpose of this paper is to take a first step in this direction and compare the fixed-order NLO QCD predictions with parton-shower-based results for the $pp \to t\bar{t}t\bar{t} + X$ process in the 4ℓ channel, thus, concentrating on the following final state $\ell^-\bar{\nu}_\ell\ell^+\nu_\ell\ell^-\bar{\nu}_\ell\ell^+\nu_\ell b\bar{b}b\bar{b}$, where $\ell^\pm = e^\pm, \mu^\pm$. For the fixed-order NLO QCD results, theoretical predictions from Ref. [10] will be used. For predictions based on parton showers, we will build on the results presented in Ref. [9] for the 1ℓ decay channel, which are based on the Powheg matching scheme, and generate new results for the 4ℓ decay channel from scratch. In addition, we will provide theoretical predictions for the $pp \to t\bar{t}t\bar{t} + X$ process matched to parton showers using the MC@NLO matching scheme. Finally, we will analyze the impact of including the so-called matrix element corrections in the top-quark decays in both predictions matched to parton showers.

The paper is organized as follows. In Sec. II, we outline the computational setup used in our study as well as highlight the differences between various theoretical approaches. In Sec. III, we present our results. This section is divided into two parts: theoretical predictions for the integrated (fiducial) cross sections and predictions for the various dimensionful and dimensionless observables that will be measured at the LHC. We summarize our results in Sec. IV, where we also provide our final conclusions.

II. DESCRIPTION OF THE CALCULATION

In this study, we consider the production and decay of four top quarks at NLO in QCD for the LHC center-of-mass energy of $\sqrt{s} = 13.6$ TeV. We provide both fixed-order predictions and results obtained from matching the NLO QCD calculation for the $pp \to t\bar{t}t\bar{t}$ process to parton showers. We concentrate on the four-lepton decay channel (denoted as 4ℓ)

$$\begin{aligned} pp \to t\bar{t}t\bar{t} + X \to W^+W^-W^+W^-b\bar{b}b\bar{b} \\ + X \to \ell^-\bar{\nu}_\ell\ell^+\nu_\ell\ell^-\bar{\nu}_\ell\ell^+\nu_\ell b\bar{b}b\bar{b} + X, \end{aligned} \quad (1)$$

where $\ell \in \{e, \mu\}$. The SM parameters are fixed according to the G_μ scheme, with the Fermi constant given by

$$G_\mu = 1.166378 \times 10^{-5}\ \text{GeV}^{-2}, \quad (2)$$

and with masses for the electroweak gauge bosons set to

$$m_W = 80.379\ \text{GeV}, \qquad m_Z = 91.1876\ \text{GeV}. \quad (3)$$

The electromagnetic coupling, α, is then evaluated according to

$$\alpha_{G_\mu} = \frac{\sqrt{2}}{\pi} G_F m_W^2 \left(1 - \frac{m_W^2}{m_Z^2}\right). \quad (4)$$

The fixed-order calculations are performed in the five-flavor scheme, which accommodates massless bottom quarks that are not decoupled from the parton density functions (PDFs). The proton content is parametrized using the MSHT20 PDF sets [12] provided by the LHAPDF library [13]. The top-quark mass is set to

$$m_t = 172.5\ \text{GeV}. \quad (5)$$

We keep the Cabibbo-Kobayashi-Maskawa matrix diagonal throughout the calculation. The final-state jets are constructed with the anti-k_T jet algorithm [14], with a clustering parameter R set to $R = 0.4$. We require the

presence of exactly four charged leptons and at least four b jets. We impose the following cuts on the transverse momentum, the rapidity, and the angular separation of the b jets:

$$p_T(b) > 25 \text{ GeV}, \qquad |y(b)| < 2.5, \qquad \Delta R_{bb} > 0.4. \quad (6)$$

In order to ensure well-observable isolated (charged) leptons in the central-rapidity region of the ATLAS and CMS detectors, we additionally require

$$p_T(\ell) > 25 \text{ GeV}, \qquad |y(\ell)| < 2.5, \qquad \Delta R_{\ell\ell} > 0.4. \quad (7)$$

Finally, we do not set any constraint on the missing transverse momentum coming from the four neutrinos. The applied cuts are motivated by the experimental analyses from ATLAS [1] and CMS [2].

As the main purpose of this article is to compare the fixed-order NLO QCD predictions with the NLO QCD results matched to parton showers, in what follows, we will focus on describing these methods and providing additional input parameters that have not yet been described, as well as pointing out the differences between various modeling approaches.

A. Fixed-order predictions

The NLO QCD corrections to the $pp \to t\bar{t}t\bar{t}$ process in the 4ℓ channel are calculated with the help of the narrow-width approximation (NWA) [10]. In this approximation, only Feynman diagrams with four top quarks are taken into account in the calculation. We neglect triple-, double-, single-, and nonresonant top-quark contributions and do not include the Breit-Wigner propagator for the top quarks or $W^{\pm}$ gauge bosons. The NLO QCD corrections are included for both the $t\bar{t}t\bar{t}$ production stage and in all top-quark decays. We present the results following the NWA-expanded prescription of the calculation (denoted as NWA_{exp}), where the cross section is given by

$$d\sigma^{\text{NLO}}_{\text{exp}} = d\sigma^{\text{NLO}}_{\text{full}} \times \left(\frac{\Gamma^1_t}{\Gamma^0_t}\right)^4 - d\sigma^{\text{LO}} \times \frac{4(\Gamma^1_t - \Gamma^0_t)}{\Gamma^0_t}. \quad (8)$$

Here, $d\sigma^{\text{NLO}}_{\text{full}}$ is the expression for the full NLO QCD calculation, where Γ_t is not treated in a perturbative manner

$$\begin{aligned} d\sigma^{\text{NLO}}_{\text{full}} = {} & d\sigma^1 \times \frac{d\Gamma^0_t}{\Gamma^1_t} \times \frac{d\Gamma^0_{\bar{t}}}{\Gamma^1_t} \times \frac{d\Gamma^0_t}{\Gamma^1_t} \times \frac{d\Gamma^0_{\bar{t}}}{\Gamma^1_t} + d\sigma^0 \times \frac{d\Gamma^1_t}{\Gamma^1_t} \times \frac{d\Gamma^0_{\bar{t}}}{\Gamma^1_t} \times \frac{d\Gamma^0_t}{\Gamma^1_t} \times \frac{d\Gamma^0_{\bar{t}}}{\Gamma^1_t} + d\sigma^0 \times \frac{d\Gamma^0_t}{\Gamma^1_t} \times \frac{d\Gamma^1_{\bar{t}}}{\Gamma^1_t} \times \frac{d\Gamma^0_t}{\Gamma^1_t} \times \frac{d\Gamma^0_{\bar{t}}}{\Gamma^1_t} \\ & + d\sigma^0 \times \frac{d\Gamma^0_t}{\Gamma^1_t} \times \frac{d\Gamma^0_{\bar{t}}}{\Gamma^1_t} \times \frac{d\Gamma^1_t}{\Gamma^1_t} \times \frac{d\Gamma^0_{\bar{t}}}{\Gamma^1_t} + d\sigma^0 \times \frac{d\Gamma^0_t}{\Gamma^1_t} \times \frac{d\Gamma^0_{\bar{t}}}{\Gamma^1_t} \times \frac{d\Gamma^0_t}{\Gamma^1_t} \times \frac{d\Gamma^1_{\bar{t}}}{\Gamma^1_t}, \end{aligned} \quad (9)$$

where σ^0, σ^1 and Γ^0, Γ^1 denote LO and NLO contributions to the $t\bar{t}t\bar{t}$ production and top-quark decay, respectively. They are computed with the NLO MSHT20 PDF set and NLO input parameters. Treating the W gauge bosons in the NWA, we can further write

$$d\Gamma_t = d\Gamma(t \to bW) \sum_{\ell\nu_\ell} \frac{d\Gamma(W \to \ell\nu_\ell)}{\Gamma_W}. \quad (10)$$

We also generate the results with the LO top-quark decays only (denoted as $\text{NWA}_{\text{LOdec}}$). This approach is motivated by the fact that the $pp \to t\bar{t}t\bar{t}$ process used for the parton-shower-based results is also generated with the LO top-quark decays. The cross section for the $\text{NWA}_{\text{LOdec}}$ case is defined as

$$d\sigma^{\text{NLO}}_{\text{LOdec}} = d\sigma^1 \times \frac{d\Gamma^0_t}{\Gamma^0_t} \times \frac{d\Gamma^0_{\bar{t}}}{\Gamma^0_t} \times \frac{d\Gamma^0_t}{\Gamma^0_t} \times \frac{d\Gamma^0_{\bar{t}}}{\Gamma^0_t}. \quad (11)$$

The fixed-order results are produced within the Helac-NLO framework [15] that comprises Helac-1Loop [16–18] and Helac-Dipoles [19–21]. They are stored in the modified Les HouchesEvent Files [22] and converted to the more compact RootNtupleFiles [23,24], which are then reweighed and analyzed with the help of the HEPlot program [25].

We employ the following decay widths for the unstable particles:

$$\Gamma_W = 2.0972 \text{ GeV}, \qquad \Gamma^{\text{NLO}}_t = 1.3535983 \text{ GeV}, \qquad \Gamma^{\text{LO}}_t = 1.4806842 \text{ GeV}. \quad (12)$$

We use a dynamical scale setting for the renormalization scale, μ_R, and factorization scale, μ_F, given by $\mu_R = \mu_F = \mu_0 = E_T/4$, where E_T is defined according to

$$E_T = \sum_{i \in \{t,\bar{t},t,\bar{t}\}} \sqrt{m_i^2 + p_T^2(i)}\,. \quad (13)$$

In Eq. (13), the momenta of the top and antitop quarks are reconstructed from their decay products. In order to estimate the theoretical uncertainties arising from neglected higher-order terms in the perturbative expansion, we use the seven-point scale variation in which μ_R and μ_F are varied independently in the range:

$$\frac{1}{2}\mu_0 \le \mu_R, \qquad \mu_F \le 2\mu_0, \qquad \frac{1}{2} \le \frac{\mu_R}{\mu_F} \le 2. \quad (14)$$

This leads to the following seven pairs that are taken into account in the error estimation:

$$\left(\frac{\mu_R}{\mu_0}, \frac{\mu_F}{\mu_0}\right) = \{(2,1),(0.5,1),(1,2),(1,1),(1,0.5),(2,2),(0.5,0.5)\}. \quad (15)$$

In practice, we look for the minimum and maximum of the obtained cross-section results to provide the final estimate of the theoretical error resulting from scale dependence.

B. NLO calculation matched to parton showers

The results are simulated using Monte Carlo (MC) event generators based on the $pp \to t\bar{t}t\bar{t} + X$ process, supplemented with parton-shower programs. The matrix element generation for the $pp \to t\bar{t}t\bar{t} + X$ process is performed either within the Powheg-Box framework [26–28] or with the help of the MadGraph5_aMC@NLO program employing the MC@NLO matching procedure for matching NLO order QCD calculations with parton showers [29]. NLO QCD theoretical predictions are generated with LO top-quark and W gauge-boson decays. In both approaches, the generated events are showered via Pythia 8.3 [30] and analyzed using the Rivet [31,32] framework, which includes an interface to the HepMC3 event record library [33] and to the FastJet library for jet finding [34,35]. In addition, the effects of taking into account the matrix element corrections in top-quark decays are investigated; see, e.g., Refs. [36,37]. Finally, hadronization, multiparton interactions, and QED showers are not addressed in this work.

1. The MC@NLO method

For the MC@NLO-type matching, the $pp \to t\bar{t}t\bar{t}$ process at NLO in QCD is generated with the help of the MadGraph5_aMC@NLO Monte Carlo program [4]. The renormalization, factorization, and matching scales are chosen at this point based on the on-shell top-quark momenta. The dynamical scale setting $\mu_R = \mu_F = \mu_0 = E_T/4$ is employed, where the value of E_T is computed according to

$$E_T = \sum_{i \in \{t,\bar{t},t,\bar{t},j\}} \sqrt{m_i^2 + p_T^2(i)}\,. \quad (16)$$

The μ_R and μ_F scales are varied according to Eq. (15). The matching in the MC@NLO scheme depends crucially on the choice of the initial shower scale μ_Q, which controls the available phase space for subsequent parton shower emissions and therefore can have a strong impact on the shower evolution. We keep the MadGraph5_aMC@NLO default choice of $\mu_Q = E_T/2$. We study the dependence on this scale by varying it by a factor of 2 up and down around the central value μ_Q. The LO decays of the top quarks and the W bosons are included via MadSpin [38]. The program in its default mode, which we retain, follows the approach described in Ref. [39]. The decay widths of the unstable particles are calculated in the MadSpin framework from the input masses and couplings at LO accuracy

$$\Gamma_W = 2.0448 \text{ GeV}, \qquad \Gamma_t = 1.4807 \text{ GeV}. \quad (17)$$

As a result, we get the following branching ratio for the W gauge boson:

$$\mathcal{BR}(W \to \ell\nu) = \sum_{i=1}^{3} \frac{\Gamma(W \to \ell_i \nu_i)}{\Gamma_W} = 0.3332844. \quad (18)$$

2. The Powheg method

The Powheg results are generated following the implementation presented in Ref. [9]. Similar to the MC@NLO approach, the $pp \to t\bar{t}t\bar{t}$ process is generated at the NLO QCD level, while the top-quark decays are considered only at LO. More precisely, we use the method described in Ref. [39] to preserve the spin correlations and introduce a smearing of top-quark and W boson virtualities according to the Breit-Wigner distributions. The same dynamical scale setting is used for μ_R and μ_F as given in Eq. (16). The matching procedure in the Powheg approach relies on the following two damping parameters: h_{damp} and h_{bornzero}; see, e.g., Ref. [40]. The h_{damp} parameter can either be set to a constant value or to a function of the underlying Born kinematics. On the other hand, h_{bornzero} is a dimensionless parameter. Both damping parameters are used to define a jet function that classifies the soft and hard real contributions. We follow Ref. [9] and set these parameters to

$$h_{\text{damp}} = \frac{E_T}{4}, \qquad h_{\text{bornzero}} = 5. \quad (19)$$

The impact of different choices of damping parameters is estimated by the five-point matching-scale variation, which corresponds to the calculation of the following contributions:

$$(h_{\text{damp}}, h_{\text{bornzero}}) = \left\{\left(\frac{E_T}{4}, 5\right), \left(\frac{E_T}{4}, 2\right), \left(\frac{E_T}{4}, 10\right), \left(\frac{E_T}{8}, 5\right), \left(\frac{E_T}{2}, 5\right)\right\}. \quad (20)$$

In addition, the initial shower scale is assigned to the transverse momentum of the extra emission generated in the event.

The top-quark and W gauge boson decay widths are evaluated at NLO in QCD, taking into account finite-width effects of the W gauge boson. Their values are given by

$$\Gamma_W = 2.0972 \text{ GeV}, \qquad \Gamma_t = 1.33254 \text{ GeV}. \quad (21)$$

The branching ratio for the leptonic decay of the W gauge boson is set to

$$\mathcal{BR}(W \to \ell\nu) = 0.325036. \quad (22)$$

It is worth mentioning here that the branching ratio and the W gauge-boson width are independent parameters in the Powheg framework. Changing the value of Γ_W will have a small impact on the results since it only enters the Breit-Wigner distributions, which are responsible for the momentum mapping between on-shell and off-shell momenta of the W decay products. The same applies to the dependence on the top-quark width Γ_t.

3. Matrix element corrections

To correct for lack of higher-order QCD effects in top-quark decays in the parton-shower-based computations, we employ the matrix element corrections (MEC). We apply the MEC according to the prescription given in Ref. [36]. This allows us to avoid the double-counting problem, i.e., generation of emissions already accounted for at the matrix-element level. Specifically, the following settings are employed in our studies:

```
SpaceShower:MEcorrections = off
TimeShower:MEcorrections = on
TimeShower:MEextended = off,
```

where `SpaceShowers` and `TimeShower` refer to initial- and final-state radiation, respectively. The `TimeShower:MEextended` flag, which is responsible for employing the MEC also for $1 \to n$ and $2 \to n$ processes, is switched off. With this flag on, the Pythia program would attempt to approximate the MEC for the whole $pp \to t\bar{t}t\bar{t}$ processes for which no exact MEC exist. Enabling the extended MEC would therefore mean that the approximate MEC would be used also in the production phase. This is a situation we would like to avoid as it would lead to double counting since NLO corrections to the production process are already incorporated in the calculation. When this flag is off, only the original splitting kernel for the emission in the $t \to bW$ decay is corrected by means of the $t \to bWg$ tree-level matrix element. It should be noted, however, that the double-counting problem can only occur in MC@NLO type simulations. In the case of Powheg, we could also include the MEC in the production stage of the $pp \to t\bar{t}t\bar{t}$ process since the hardest emission in the production is always guaranteed to be generated prior to showering. In this case, the impact of the production MEC would therefore be limited to only small p_T regions, where the cross section is Sudakov suppressed, and the emissions generated by Powheg do not occur. As a result, the production MEC are essentially negligible in Powheg and may or may not be included. Nevertheless, we decided to use the same settings for the Powheg and MC@NLO matching results.

In addition, one can switch on the MEC to emissions after the first one via the following flag:

```
TimeShower::MEafterFirst = on.
```

We leave this flag enabled as it is the default setting in Pythia. This would correspond, for example, to two consecutive corrected emissions from the b quark, i.e., to such a process $t \to Wbg(g \to gg) \to Wbgg$. We refer to this setup as $\oplus$ MEC. However, we also investigate the case where the use of the MEC is not allowed after the first emission. This can be achieved by setting

```
TimeShower::MEafterFirst = off.
```

We refer to this setting as $\oplus$ MEC$^{1\text{st}}$. We expect the difference between $\oplus$ MEC and $\oplus$ MEC$^{1\text{st}}$ to be very small. We plan to check this for one type of matching, namely the MC@NLO matching.

C. Differences in the various approaches

Below we highlight the differences in the approaches described so far. Leaving aside the fact that the NLO plus parton shower results provide predictions with (soft/collinear) emissions included to all orders via repeated branching of quarks and gluons, here we will rather focus on the differences that arise in the calculations of the $pp \to t\bar{t}t\bar{t} + X$ process in the 4ℓ decay channel. Such differences contribute to the systematic uncertainties for this process.

In the case of fixed-order NLO QCD predictions, following the NWA$_{\text{exp}}$ approach, higher-order QCD corrections are consistently included in both the production and decay stages of the $pp \to t\bar{t}t\bar{t} + X$ process. Furthermore, spin correlations at the NLO level are preserved throughout the calculation. On the other hand, in the NWA$_{\text{LOdec}}$ results, only LO top-quark decays are present, and therefore, only LO spin correlations are considered. Finally, although in the parton-shower-based predictions, the higher-order QCD corrections in top-quark decays are approximately taken into account, formally spin correlations are only LO accurate. Since the kinematics of the top-quark decay products are influenced by spin correlations, it is important to investigate the effects of higher-order corrections in the decays and to examine precisely to what extent parton showers can mimic these effects in order to fully understand the obtained results.

Another difference concerns the choice of the scale setting used for μ_R and μ_F. In the fixed-order approach, we define the dynamical scale setting via Eq. (13), where the

additional light jet from the real emission part of the NLO calculation, if present, is excluded from the sum. In contrast, the scale setting defined in Eq. (16), used in both parton-shower-based computations, includes the additional light jet. We note here that it is not possible to achieve one-to-one correspondence in the scale setting between the fixed-order and parton-shower-based predictions. In the former case, the scale setting is based on the observed final states (leptons and jets), where the momenta of the top and antitop quarks are reconstructed from their decay products in the fiducial phase-space regions. In the latter case, the scale setting is based solely on the stable top quarks and extra jet. Unlike the fixed-order case, this additional jet can only come from the production stage of the process. Thus, different scaling settings can be considered as part of the systematic uncertainties.

A further distinction comes from the fact that the fixed-order NLO calculations depend on the chosen values of the t-quark and W-boson widths, as seen in Eqs. (8) and (10). The cross section for the parton-shower matched calculations is instead given in terms of the production cross section times the corresponding branching ratios

$$d\sigma_{4\ell}^{\mathrm{NLO+PS}} = d\sigma_{pp\to t\bar{t}t\bar{t}}^{\mathrm{NLO}} \times \left[\mathcal{BR}(t \to W^+ b)\mathcal{BR}(\bar{t} \to W^- \bar{b})\right]^2 \times 16\left[\mathcal{BR}(W^\pm \to \ell\nu)\right]^4, \tag{23}$$

where the factor 16 accounts for all the combinations of the leptonic $W^\pm$ decays with $\ell = e$, μ, and $\mathcal{BR}(W^\pm \to \ell\nu)$ refers to a given lepton flavor. Since the CKM matrix is kept diagonal in our calculations, we can write $\mathcal{BR}(t \to W^+ b) = \mathcal{BR}(\bar{t} \to W^- \bar{b}) = 1$. Consequently, the dependence of $d\sigma_{4\ell}^{\mathrm{NLO+PS}}$ on the top-quark width vanishes. On the contrary, we are sensitive to $\mathcal{BR}(W^\pm \to \ell\nu)$. In MadSpin, all branching ratios are calculated with LO accuracy based on the given input parameters. On the other hand, in Powheg, $\mathcal{BR}(W^\pm \to \ell\nu)$ is an independent input parameter that we set to the NLO value. Although the difference between the total leptonic W boson branching ratio at LO and NLO is only 2.5%, the cross section depends on $\mathcal{BR}(W^\pm \to \ell\nu)$ quadruply. This increases the cross section by ∼10% when LO branching factors are used instead. To consistently compare both approaches, we globally rescaled the results obtained within the Powheg framework by

$$\left(\frac{\mathcal{BR}^{\mathrm{LO}}(W \to \ell\nu)}{\mathcal{BR}^{\mathrm{NLO}}(W \to \ell\nu)}\right)^4 = \left(\frac{1/3}{\mathcal{BR}^{\mathrm{NLO}}(W \to \ell\nu)}\right)^4 = 1.106087. \tag{24}$$

The final conceptual difference between the fixed-order computations and the parton-shower matched predictions concerns the definition of the b jets in the final state. The fixed-order calculations are performed in the five-flavor scheme with massless bottom quarks. We employ the charge-blind b jet tagging, see, e.g., Ref. [41]. In practice, the following set of recombination rules is used:

$$bg \to b, \quad \bar{b}g \to \bar{b}, \quad b\bar{b} \to g, \quad bb \to g, \quad \bar{b}\,\bar{b} \to g, \tag{25}$$

which makes the jet-flavor definition infrared safe at NLO in QCD. On the contrary, in the parton-shower matched simulations, the b quark is treated as a massive quark, and the collinear divergence in the $g \to b\bar{b}$ splitting is regulated by the mass of the bottom quark. Thus, in this case, a b jet is always defined as a jet that has at least one b quark among its constituents. Note here that this is actually closer to what is done experimentally, where the definition of b jets is based on the presence of intermediate heavy long-lived b-flavored hadrons decaying at displaced vertices.

We would also like to add here that precise identification of b jets can pose serious infrared and collinear safety problems for predictions beyond NLO in QCD. In such a case, the so-called flavored anti-k_T jet algorithms should be used instead; see, e.g., Refs. [42–44] and the comparative study presented in Ref. [45]. Moreover, the flavored anti-k_T jet algorithms might be applied to parton-shower-based predictions to check whether the obtained cross-section results contain large logarithms of the type $\log(m_b/p_{T,b})$. To ensure the robustness of our parton-shower-based predictions, we also generated the integrated and differential cross-section predictions using a flavored IR safe anti-k_T jet algorithm that is available as a FastJet Plugin.[1] All the differences at the integrated and differential cross-section level that we found were significantly lower than the corresponding theoretical uncertainties obtained using a scale variation procedure.

III. NUMERICAL RESULTS

In our study of the $pp \to t\bar{t}t\bar{t} + X$ process in the 4ℓ decay channel, we require the presence of exactly four charged leptons and at least four b jets in the final state. In practice, however, for the fixed-order NLO QCD calculation, we can only have up to five b jets. On the contrary, in the parton-shower matched predictions, we can easily observe up to 10 or even 11 b jets. Moreover, in this case, the four b jets with the highest p_T do not always correspond to the b jets generated in the top-quark decays. Understanding the origin of b jets is particularly important when the identification of b jets from top-quark decays is required, which can be the case, for example, when extrapolating the fiducial measurement to the full phase space in order to unfold to stable top quarks or when the $pp \to t\bar{t}t\bar{t} + X$ process is treated as one of the background processes in the search for new physics. Therefore, in addition to the general comparison of the four hardest b jets

[1] https://github.com/jetflav/IFNPlugin.

TABLE I. Integrated fiducial cross-section predictions at NLO in QCD for the $pp \to t\bar{t}t\bar{t} + X$ process in the 4ℓ channel. We present the fixed-order results and predictions matched to parton shower. For the fixed-order case, we provide the results for $\sigma^{\mathrm{NLO}}_{\mathrm{NWA}_{\mathrm{exp}}}$ and for $\sigma^{\mathrm{NLO}}_{\mathrm{NWA}_{\mathrm{LO_{dec}}}}$. The parton-shower-based results are presented without and with the b jet identification as well as for the various MEC settings. The scale uncertainties, δ^{scale}, and parton-shower matching uncertainties, δ^{match}, are also reported.

THEORETICAL APPROACH	σ [ab]	$+\delta^{\mathrm{scale}}$	$-\delta^{\mathrm{scale}}$	$+\delta^{\mathrm{match}}$	$-\delta^{\mathrm{match}}$	$\sigma/\sigma_{\mathrm{NWA}_{\mathrm{exp}}}$
Fixed-order NLO						
$\mathrm{NWA}_{\mathrm{exp}}$	5.170(3)	+12%	−20%	⋯	⋯	1.0000
$\mathrm{NWA}_{\mathrm{LO_{dec}}}$	5.646(3)	+22%	−23%	⋯	⋯	1.0921
NLO + PS without b jet identification						
MC@NLO + PS	4.891(8)	+15%	−21%	+1.1%	−0.7%	0.9460
MC@NLO + PS ⊕ $\mathrm{MEC}^{1\mathrm{st}}$	5.081(8)	+15%	−21%	+0.9%	−0.6%	0.9828
MC@NLO + PS ⊕ MEC	5.098(8)	+15%	−21%	+0.7%	−0.5%	0.9861
POWHEG + PS	4.820(6)	+15%	−21%	+0.0%	−0.5%	0.9323
POWHEG + PS ⊕ MEC	5.024(6)	+15%	−21%	+0.0%	−0.5%	0.9718
NLO + PS with b jet identification						
MC@NLO + PS	4.708(7)	+15%	−21%	+0.8%	−0.4%	0.9106
MC@NLO + PS ⊕ $\mathrm{MEC}^{1\mathrm{st}}$	4.910(8)	+15%	−21%	+0.6%	−0.4%	0.9497
MC@NLO + PS ⊕ MEC	4.923(8)	+15%	−21%	+0.5%	−0.5%	0.9522
POWHEG + PS	4.656(6)	+15%	−21%	+0.1%	−0.2%	0.9006
POWHEG + PS ⊕ MEC	4.865(6)	+15%	−21%	+0.0%	−0.2%	0.9410

from the fixed-order predictions with those from the NLO plus parton-shower simulations, in the latter case, we will also attempt to identify the b jets originating directly from the top-quark decays. This can be achieved by exploiting the so-called mother-daughter history available within the Pythia framework from the production vertex to a given final state; see, e.g., Ref. [30]. The b jets produced at the matrix-element level can originate not only from the resonant top quarks, but also from the real-emission part of the NLO QCD calculations, e.g., from the following subprocesses $gb/bg \to t\bar{t}t\bar{t}b$ and $g\bar{b}/\bar{b}g \to t\bar{t}t\bar{t}\,\bar{b}$. However, such contributions are small, of the order of 0.2%, and are therefore disregarded. Thus, we identify a b jet from the matrix-element calculation as a jet that contains a bottom quark coming either from t or $\bar{t}$. Any b quark originating from a $g \to b\bar{b}$ splitting is excluded. We then require that, among all b jets in the event, there are always exactly four such b jets present, and only these events are taken into account when constructing integrated and differential cross-section predictions labeled as the NLO plus parton shower predictions (NLO + PS) with the b jet identification.

A. Integrated cross-section predictions

We start by presenting and comparing the integrated fiducial cross-section predictions for the $pp \to t\bar{t}t\bar{t} + X$ process in the 4ℓ decay channel together with their corresponding theoretical uncertainties. In particular, we provide theoretical uncertainties estimated from independent variations of the renormalization and factorization scales. For the parton-shower-based predictions, we also show the parton-shower matching uncertainties. For the results obtained with the MC@NLO matching, the latter uncertainties are estimated by a variation of the initial shower scale μ_Q, whereas for the Powheg case, the variation of the two damping parameters is performed instead.

Our findings are summarized in Table I. Several statements are in order now. Firstly, all parton-shower-based predictions are smaller than the fixed-order results. Indeed, in the presence of multiple shower emissions, the parton shower allows the b jets to evade kinematical bounds that would be otherwise present at the fixed-order case. Moreover, omitting NLO QCD corrections in top-quark decays increases not only the value of the integrated cross section by about 9%, but also the size of the theoretical uncertainties arising from scale dependence from 20% to 23%. The NLO plus parton shower predictions without any MEC and b jet identification differ from the default $\sigma^{\mathrm{NLO}}_{\mathrm{NWA}_{\mathrm{exp}}}$ fixed-order result by −5% and −7% for the MC@NLO and Powheg prediction, respectively. Nevertheless, these differences are well within the quoted theoretical uncertainties, which are of the order of 21% for the parton-shower-based predictions.

Secondly, when the b jet identification is used, about 3%–5% more events are vetoed. This simply means that there might be b jets from parton showers that undergo selection cuts and easily mimic the b jets from the top-quark decays. The latter, due to multiple emissions of light

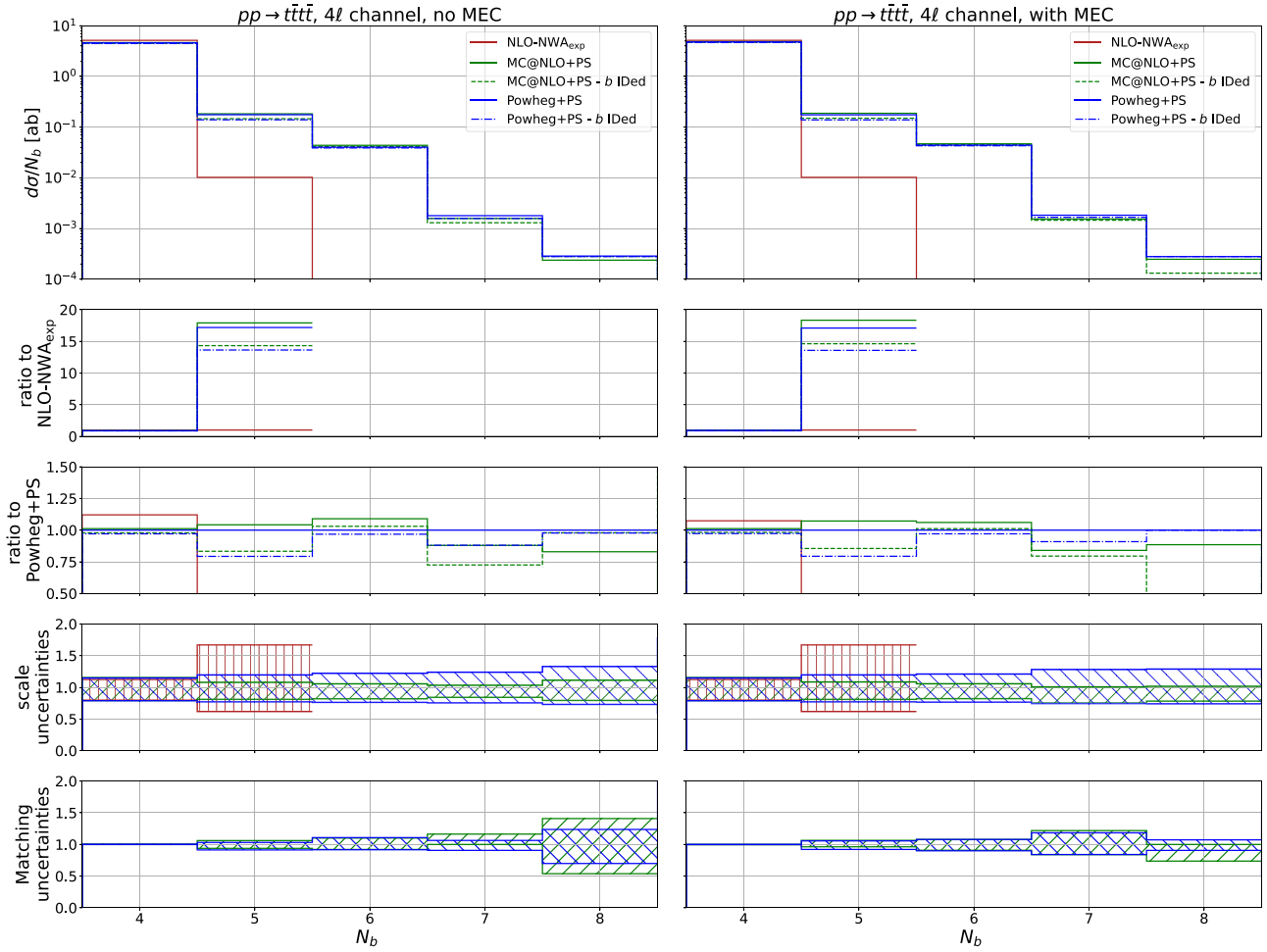


FIG. 1. Integrated fiducial cross-section predictions at NLO in QCD for the $pp \to t\bar{t}t\bar{t} + X$ process in the 4ℓ channel as a function of the number of b jets present. The parton-shower-based results are given without (left) and with the MEC (right). Predictions without (solid line) and with (dashed line) the b jet identification are also shown. The second panel from the top provides the ratio to the fixed-order results. The third panel shows the ratio to the Powheg predictions. The fourth panel presents the scale uncertainties, and the bottom panel depicts the parton-shower matching uncertainties.

jets, no longer pass the required cuts. This leads to differences of up to 10% with respect to $\sigma^{\mathrm{NLO}}_{\mathrm{NWA_{exp}}}$.

Thirdly, we note that including the MEC in the top-quark decays increases the integrated fiducial cross section by about 4%–5% regardless of whether the b jet identification is used. Moreover, as expected, the difference between the two results $\oplus$ MEC$^{1\mathrm{st}}$ and $\oplus$ MEC is less than 1%. Overall, the inclusion of the MEC leads to better agreement with the fixed-order $\mathrm{NWA_{exp}}$ result, highlighting the importance of the MEC in parton-shower-based predictions.

We can further observe that the NLO QCD parton-shower-based predictions for the $pp \to t\bar{t}t\bar{t} + X$ process in the 4ℓ channel, as obtained with the MC@NLO and Powheg matching methods, are in a rather good agreement.

It is interesting to see the results for the particular number of the b jets. To this end, in Fig. 1, we present the integrated fiducial cross-section predictions at NLO in QCD as a function of the number of final state b jets. Each bin indicates the cross-section result with the exact number of b jets. The parton-shower-based results are given without and with the MEC as well as without and with the b jet identification. The second panel from the top shows the ratio to the fixed-order predictions. The third panel presents the ratio to the Powheg results. This way, we can better observe the spread of the parton-shower-based results for high b jet multiplicities. The fourth panel depicts the theoretical uncertainties obtained by scale variation, whereas the lower panel provides the parton-shower matching uncertainties. Since the fixed-order NLO QCD predictions only include up to five b jets, the first bin is NLO accurate, the second bin LO accurate, and starting from $N_b = 6$, the b jets are described solely by the shower evolution. The cross section with exactly four b jets gives the dominant contribution to the integrated cross section for the $pp \to t\bar{t}t\bar{t} + X$ process in the 4ℓ channel. In this bin, the NLO plus parton-shower predictions are smaller than the NLO

QCD fixed-order results by about 10%. This difference is, however, well within the shown scale uncertainties, which are of the order of 20%. On the other hand, for the case with exactly five b jets, the parton-shower-based predictions are up to 19 times larger than the fixed-order result. Moreover, the increased theoretical uncertainties in the latter case reflect its LO nature. In addition, we can observe that the various NLO plus parton showers results agree with each other within the given scale uncertainties. As the number of the b jets increases, the size of the scale and matching uncertainties increases as well. For a large number of b jets, they become of similar size, especially if the MEC are not applied.

Before we turn to the differential cross-section results, let us briefly note that in this study, we do not analyze the PDF uncertainty. This is because they have already been discussed in detail in Ref. [10] for the fixed-order NLO QCD predictions. Nevertheless, for the sake of completeness, we would like to state that the PDF uncertainties for the $pp \to t\bar{t}t\bar{t} + X$ process in the 4ℓ channel are up to 2% for the NNPDF3.1 PDF set [46], of the order of 3%–4% for MSHT20 (our default PDF set) and up to 5%–6% for the CT18 PDF set [47].

B. Differential cross-section predictions

In the next step, we examine various differential cross-section distributions obtained by applying the cuts and input parameters specified in Sec. II. We consider a set of both dimensionful and dimensionless observables. For dimensionful observables, the ranges are chosen to ensure the presence of at least a few events in the last bin, assuming the integrated luminosity of the HL-LHC as well as including τ leptons in the definition of leptons. We remind the reader that the HL-LHC will produce more than 250 fb^{-1} of data per year and be capable of collecting up to 4000 fb^{-1} of data during its whole exploitation period. For each of the observables illustrated in Figs. 2–5, we present four plots and divide them into two classes: the results without and with MEC. Note that the results including MEC are only provided for the case of $\oplus$ MEC since the differences between $\oplus$ MEC$^{1\text{st}}$ and $\oplus$ MEC are negligible also at the differential cross-section level. For each plot, the upper panels show the absolute NLO predictions for the various approaches we considered. In particular, we show the fixed-order NLO QCD results in the NWA as well as the two parton-shower-based predictions with and without the b jet identification. In each case, the left plots correspond to the results without MEC, while the right plots include such effects. The second panel from the top provides the ratio to the $\sigma^{\text{NLO}}_{\text{NWA}_{\text{exp}}}$ result. The third panel depicts the uncertainty bands resulting from scale variations. In this case only, the uncertainties for the predictions without the b jet identification are plotted. However, we have verified that the identification of the b jets does not change their size. Finally, the bottom panel presents the matching uncertainties for the parton-shower-based results, again only for the predictions without the b jet identification.

In Fig. 2, we show the transverse momentum of the first, $p_T(b_1)$, and second hardest b jets, $p_T(b_2)$. Prior to the application of the MEC, differences of up to 10% are visible compared to the $\sigma^{\text{NLO}}_{\text{NWA}_{\text{exp}}}$ case. Much better consistency in the shape of these distributions can be observed after the MEC are included. Indeed, in the phase-space regions where most of the events are located, the various predictions now differ by only about 5%. In addition, the shape of the $p_T(b_1)$ and $p_T(b_2)$ distributions does not change significantly after the b jet identification is performed. This indicates that the two hardest b jets most likely come from the top-quark decays. Finally, also at the differential cross-section level, the two parton-shower-based results agree with each other within the quoted theoretical uncertainties due to missing higher-order corrections. These uncertainties are of the order of 15%–20%, and thus, they are similar in size to those observed at the integrated cross-section level. In addition, the matching uncertainties are negligible. The latter effect is visible for all the observables we have examined for this process.

Next, we look at the transverse momentum distributions of the third, $p_T(b_3)$, and fourth hardest b jets, $p_T(b_4)$, that are presented in Figure 3. In contrast to $p_T(b_1)$ and $p_T(b_2)$, for $p_T(b_3)$ and $p_T(b_4)$, we can observe more significant shape distortions when comparing the various predictions. If the MEC are not employed, shape changes of up to 10%–15% are visible when parton-shower-based predictions are contrasted with the fixed-order $\sigma^{\text{NLO}}_{\text{NWA}_{\text{exp}}}$ result. These differences are reduced to less than 10% if the MEC are enabled. The increasing deviations between the results without and with the b jet identification indicate that the probability that the third and fourth hardest b jets originate from the parton-shower simulations rather than from the top-quark decays increases significantly. One can also see larger discrepancies between the two parton-shower-based predictions, especially in the case of the high p_T tails of the two distributions. This is because the emissions in MC@NLO-like simulations, unlike in Powheg simulations, are not ordered in hardness; i.e., the hardest emission is not necessarily generated before the parton shower is added. However, all presented results are consistent with each other due to relatively large theoretical uncertainties.

Turning to leptonic observables, in Fig. 4, we plot the transverse momentum of the hardest (charged) lepton, $p_T(\ell_1)$, and the missing transverse momentum due to the four neutrinos, $p_T(\text{miss})$. In the high p_T tails, parton showers have a significant impact on both observables. We observe shower effects up to even 17%. The large discrepancy between the parton-shower matched results and the fixed-order predictions in these phase-space regions can be explained by the fact that multiple parton-shower emissions decrease the transverse momenta of the color-neutral

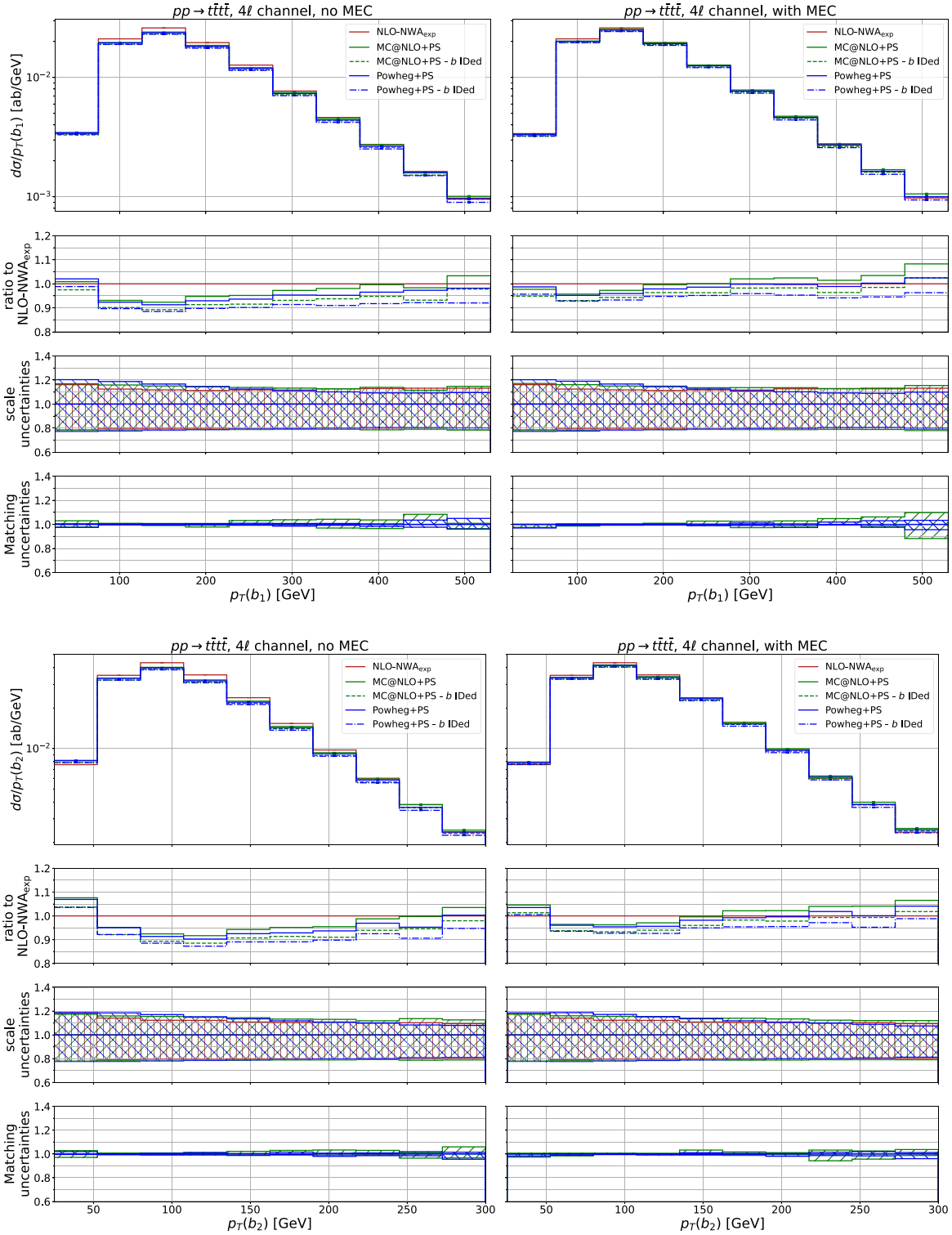


FIG. 2. Differential cross-section distributions at NLO in QCD for the $pp \to t\bar{t}t\bar{t} + X$ process in the 4ℓ channel as a function of the transverse momentum of the first and second hardest b jets, $p_T(b_1)$ and $p_T(b_2)$, respectively. The parton-shower-based results are given without (left) and with the MEC (right). Predictions without (solid line) and with (dashed line) the b jet identification are also shown. The second panel from the top provides the ratios to $\sigma^{\mathrm{NLO}}_{\mathrm{NWA}_{\mathrm{exp}}}$. The third panel depicts the scale uncertainties, and the bottom panel presents the parton-shower matching uncertainties.

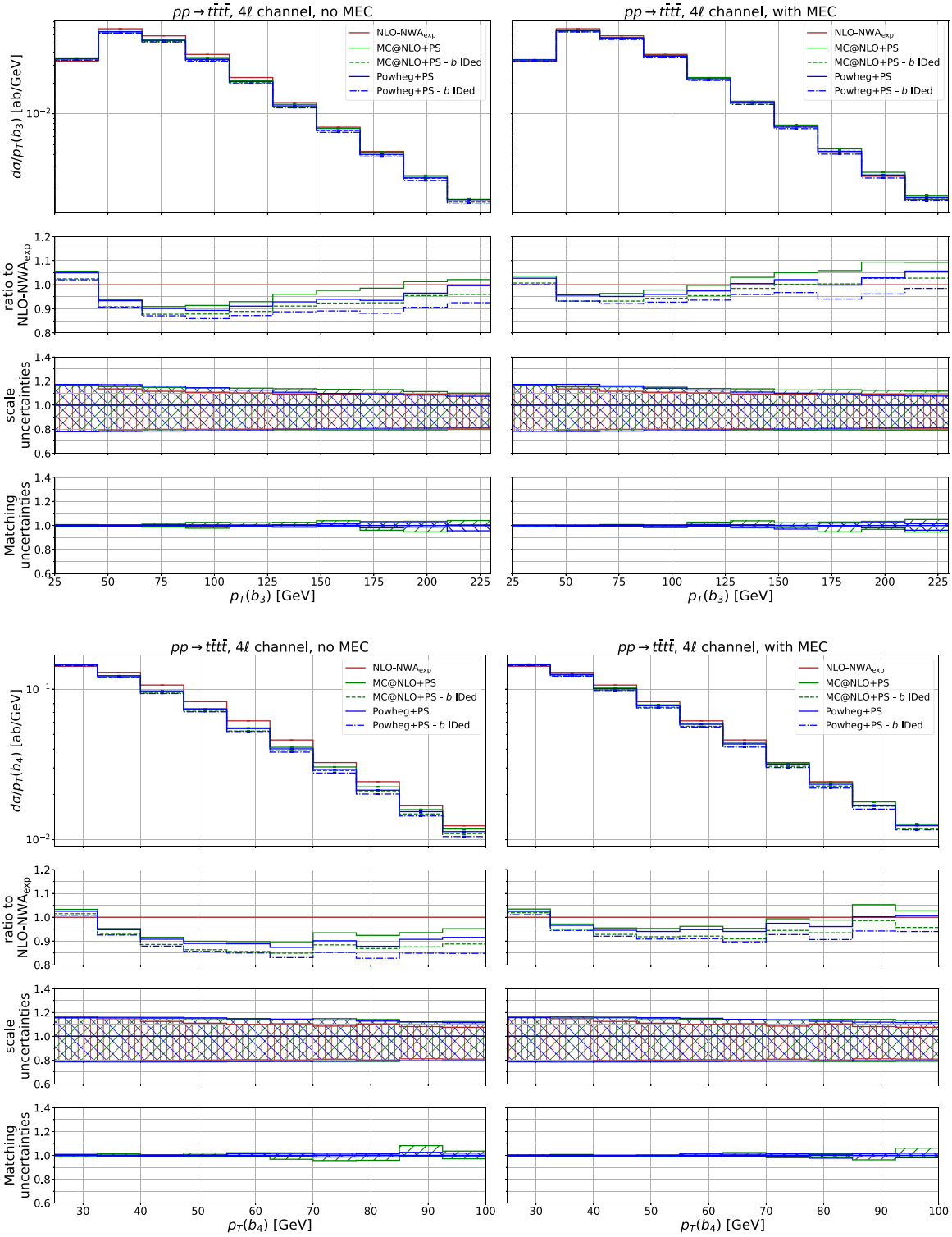


FIG. 3. Same as Fig. 2 but for the transverse momentum of the third and fourth hardest b jets, $p_T(b_3)$ and $p_T(b_4)$, respectively.

particles, which have to recoil against the sum of all emitted partons. Enabling the MEC brings the different predictions closer together. Indeed, the deviations are now reduced to about 10%.

Finally, we analyze two dimensionless distributions. In Fig. 5, we plot the rapidity of the hardest b jet, $y(b_1)$, and the angular distance between the first and second hardest charged leptons, $\Delta\phi(\ell_1\ell_2)$. The $\Delta\phi(\ell_1\ell_2)$ observable is

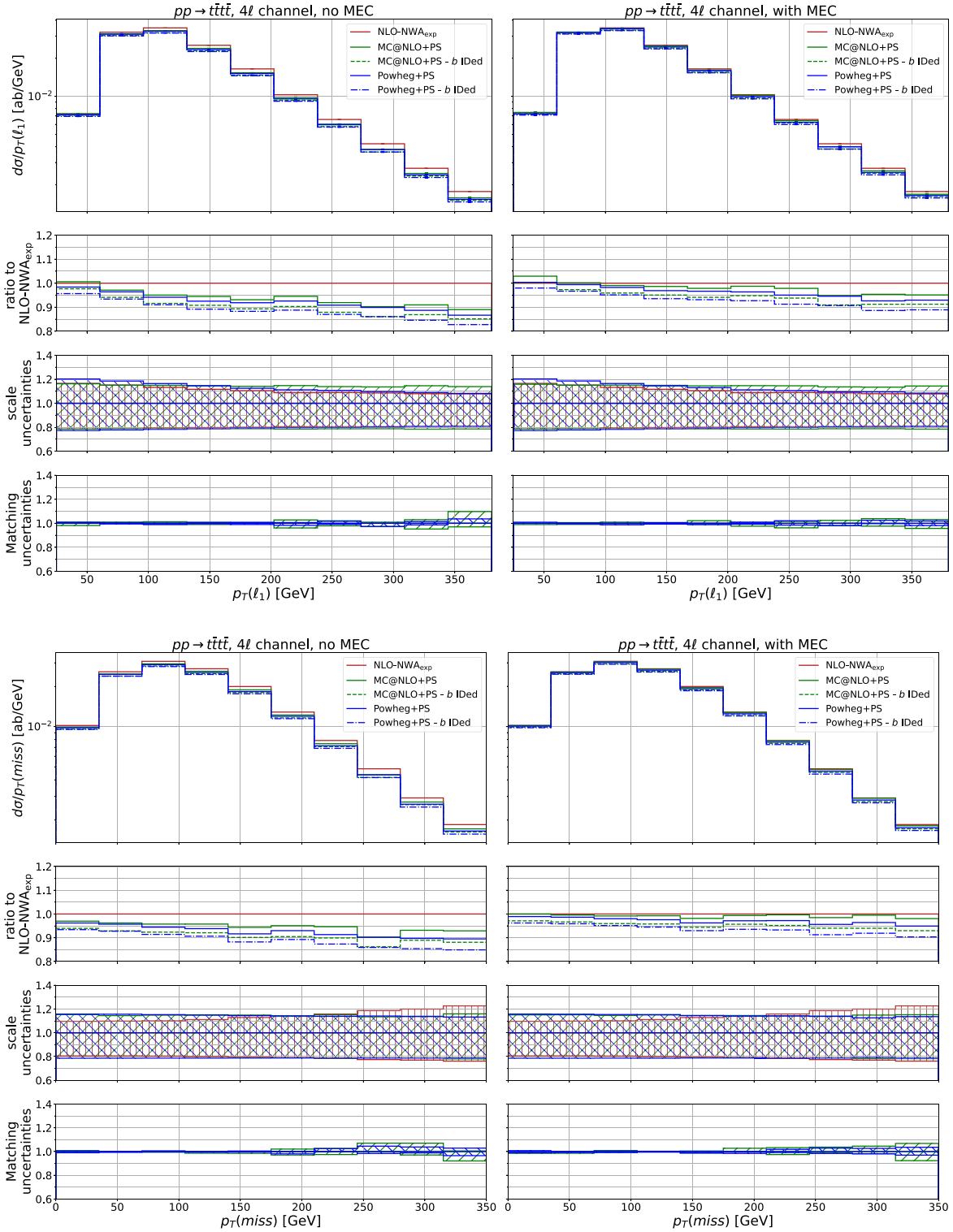


FIG. 4. Same as Fig. 2 but for the transverse momentum of the hardest charged lepton, $p_T(\ell_1)$ and for the missing transverse momentum, $p_T(\text{miss})$.

sensitive to new physical scenarios in which new heavy states can be produced that further decay into top quarks. In general, the angular distributions of charged leptons are of great importance because they reflect spin correlations and can be used to probe the $\mathcal{CP}$ quantum numbers of such new states. For both observables, we note that the ratio of the parton-shower-based predictions to fixed-order results is flat, with any differences arising solely from changes in

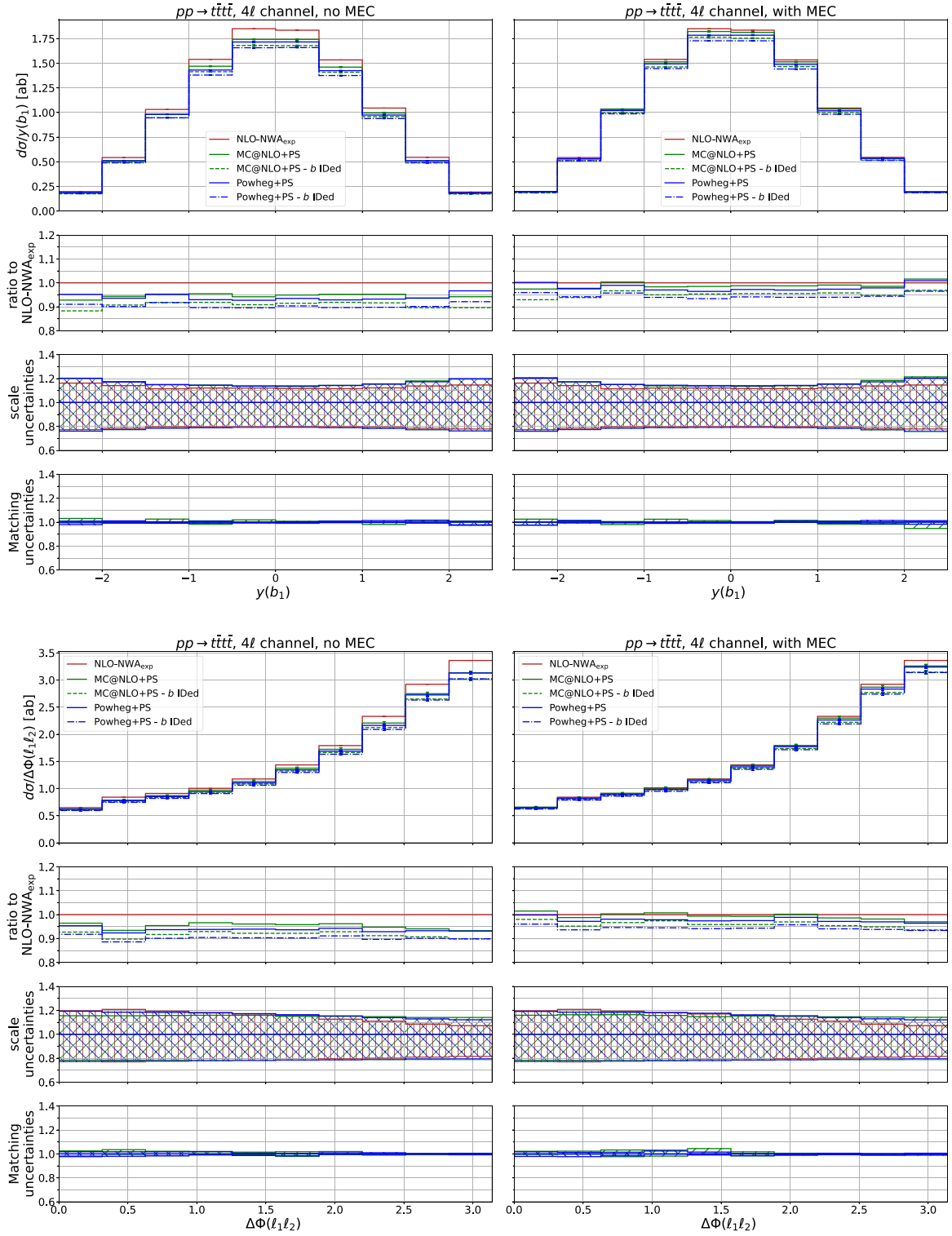


FIG. 5. Same as Fig. 2 but for the rapidity of the hardest b jet, $y(b_1)$, and the angular distance between the first and second hardest (charged) leptons, $\Delta\phi(\ell_1\ell_2)$.

normalization. We verified this explicitly by also generating the normalized differential cross-section distributions. This normalization change is in the range of 5%–10% depending on whether an attempt is made to identify the b jets from top-quark decays. Also, for these two observables, the MEC method helps to bring the different predictions closer together. The difference in the normalization factor is reduced to a value below 5%, which is within the obtained

theoretical uncertainties. Although we have only shown the rapidity of the hardest b jet here, the same conclusions can be drawn for the remaining three b jets, i.e., for $y(b_2)$, $y(b_3)$, and $y(b_4)$. Similarly, every other combination of leptons that we used to construct $\Delta\phi(\ell\ell)$ behaved similarly to the $\Delta\phi(\ell_1\ell_2)$ differential cross-section distribution for all the theoretical predictions that we considered.

IV. SUMMARY AND CONCLUSIONS

In this paper, we presented a comparison of the fixed-order NLO QCD results for the $pp \to t\bar{t}t\bar{t} + X$ process in the 4ℓ channel, with the parton-shower-based predictions obtained using the MC@NLO and Powheg matching. In the fixed-order case, all higher-order QCD effects were consistently incorporated into the production and decays of the four top quarks. This calculation was performed in the NWA, which preserves the NLO spin correlations throughout the computational process. In the second case, NLO QCD corrections were only included in the production stage of the $pp \to t\bar{t}t\bar{t} + X$ process, whereas top-quark decays were treated at LO, thus, neglecting NLO spin correlations. Furthermore, we examined the importance of using the MEC in top-quark decays for the parton-shower-based predictions. Such a multilayer comparison helped us to assess to what extent parton showers could approximate the higher-order QCD effects in top-quark decays. We investigated the validity of these approximations in such a complex environment, both at the integrated and differential cross-section level. Finally, the presented comparison allowed us to identify observables and specific phase-space regions that are sensitive to the resummed dominant soft-collinear logarithmic corrections from parton showers, which are not present in the fixed-order NLO QCD predictions.

To conclude, at the integrated cross-section level, all the parton-shower-based results were smaller than the predictions obtained at the fixed-order level. This is due to the fact that multiple shower emissions allow the b jets originating from the matrix-element level to go below the given kinematic cut. Moreover, neglecting completely NLO QCD effects in top-quark decays increased the cross section by about 9% and the theoretical uncertainties by 3%. The Powheg and MC@NLO results recovered some of these higher-order effects. Indeed, the NLO plus parton-shower predictions differed from the $\sigma^{\mathrm{NLO}}_{\mathrm{NWA}_{\mathrm{exp}}}$ result by 5%–7%. After including the MEC, these differences were reduced to 1%–3%, highlighting the importance of enabling such effects in the parton-shower-based predictions. When trying to identify the b jets from top-quark decays, we observed that about 3%–5% more events were vetoed. As a result, the Powheg and MC@NLO predictions differed from the fixed-order result by 10%. These differences were also reduced to 5%–6% after employing the MEC. We also investigated the case where the use of the MEC was not allowed after the first parton-shower emission. As expected, the difference between the two results $\oplus$ MEC and $\oplus$ MEC$^{1\mathrm{st}}$ was very small, less than 1%. Although it was very interesting and important to understand these various differences, we must add here that at present they all fall within the estimated theoretical uncertainties, which are of the order of 20%.

In the case of differential cross-section distributions for all the observables considered, the size of the theoretical uncertainties was driven by the size of the scale uncertainties. Also, at the differential cross-section level, these uncertainties were consistently of the order of 20%. We observed that the parton-shower matching uncertainties were negligible for all the observables we analyzed. Furthermore, we could clearly notice that enabling the MEC algorithm in Pythia improved the modeling of top-quark decays in the shower evolution for all the observables we examined. Moreover, we saw good consistency between the results obtained with the Powheg and MC@NLO matching. We also examined how various differential cross-section distributions were modified by the showering stage and in particular saw that there was a significant (indirect) impact on the leptonic observables. On the contrary, similar large effects were not observed when looking, for example, at the two hardest b jets. On average, the shower emissions were softer in p_T with respect to the first and second hardest b jet from the top-quark decays. In these cases, in the high p_T tails, the obtained predictions were closer to the fixed-order NLO QCD results. This was especially visible in the case of the results obtained within the Powheg framework. Finally, another very important topic that we investigated was spin correlations. Having fixed-order predictions describing top-quark decays and spin correlations with NLO QCD accuracy, we were in an excellent position to test the impact of parton showers and MEC on the angular distributions. Overall, we observed that for these distributions, the differences between the parton-shower matched results and the fixed-order predictions were in the range of 5%–10%. Introducing the MEC helped to reduce them to less than 5%.

ACKNOWLEDGMENTS

We would like to thank Manfred Kraus for very helpful discussions regarding the results presented in Ref. [9]. This work was supported by the Deutsche Forschungsgemeinschaft (DFG) under Grant No. 396021762-TRR 257: *Particle Physics Phenomenology after the Higgs Discovery*, and grant 400140256-GRK 2497: *The Physics of the Heaviest Particles at the LHC*. Support by a grant of the Bundesministerium für Bildung und Forschung (BMBF) is additionally acknowledged. The authors gratefully acknowledge the computing time provided to them at the NHR Center NHR4CES at RWTH Aachen

University (Project No. p0020216). This is funded by the Federal Ministry of Education and Research, and the state governments participating on the basis of the resolutions of the GWK for national high performance computing at universities.

DATA AVAILABILITY

The data that support the findings of this article are not publicly available. The data are available from the authors upon reasonable request.

[1] G. Aad *et al.* (ATLAS Collaboration), Observation of four-top-quark production in the multilepton final state with the ATLAS detector, Eur. Phys. J. C **83**, 496 (2023); **84**, 156(E) (2024).

[2] A. Hayrapetyan *et al.* (CMS Collaboration), Observation of four top quark production in proton-proton collisions at $\sqrt{s} = 13$ TeV, Phys. Lett. B **847**, 138290 (2023).

[3] G. Bevilacqua and M. Worek, Constraining BSM physics at the LHC: Four top final states with NLO accuracy in perturbative QCD, J. High Energy Phys. 07 (2012) 111.

[4] J. Alwall, R. Frederix, S. Frixione, V. Hirschi, F. Maltoni, O. Mattelaer, H. S. Shao, T. Stelzer, P. Torrielli, and M. Zaro, The automated computation of tree-level and next-to-leading order differential cross sections, and their matching to parton shower simulations, J. High Energy Phys. 07 (2014) 079.

[5] F. Maltoni, D. Pagani, and I. Tsinikos, Associated production of a top-quark pair with vector bosons at NLO in QCD: Impact on tt̄H searches at the LHC, J. High Energy Phys. 02 (2016) 113.

[6] R. Frederix, D. Pagani, and M. Zaro, Large NLO corrections in $t\bar{t}W^{\pm}$ and $t\bar{t}t\bar{t}$ hadroproduction from supposedly subleading EW contributions, J. High Energy Phys. 02 (2018) 031.

[7] M. van Beekveld, A. Kulesza, and L. M. Valero, Threshold resummation for the production of four top quarks at the LHC, Phys. Rev. Lett. **131**, 211901 (2023).

[8] M. van Beekveld, A. Kulesza, M. Lupattelli, and T. Saracco, Invariant-mass threshold resummation for the production of four top quarks at the LHC, J. High Energy Phys. 10 (2025) 209.

[9] T. Ježo and M. Kraus, Hadroproduction of four top quarks in the powheg box, Phys. Rev. D **105**, 114024 (2022).

[10] N. Dimitrakopoulos and M. Worek, Four top final states with NLO accuracy in perturbative QCD: 4 lepton channel, J. High Energy Phys. 06 (2024) 129.

[11] N. Dimitrakopoulos and M. Worek, Four top final states with NLO accuracy in perturbative QCD: 3 lepton channel, J. High Energy Phys. 03 (2025) 025.

[12] S. Bailey, T. Cridge, L. A. Harland-Lang, A. D. Martin, and R. S. Thorne, Parton distributions from LHC, HERA, Tevatron and fixed target data: MSHT20 PDFs, Eur. Phys. J. C **81**, 341 (2021).

[13] A. Buckley, J. Ferrando, S. Lloyd, K. Nordström, B. Page, M. Rüfenacht, M. Schönherr, and G. Watt, LHAPDF6: Parton density access in the LHC precision era, Eur. Phys. J. C **75**, 132 (2015).

[14] M. Cacciari, G. P. Salam, and G. Soyez, The anti-k_t jet clustering algorithm, J. High Energy Phys. 04 (2008) 063.

[15] G. Bevilacqua, M. Czakon, M. V. Garzelli, A. van Hameren, A. Kardos, C. G. Papadopoulos, R. Pittau, and M. Worek, Helac-NLO, Comput. Phys. Commun. **184**, 986 (2013).

[16] G. Ossola, C. G. Papadopoulos, and R. Pittau, On the Rational Terms of the one-loop amplitudes, J. High Energy Phys. 05 (2008) 004.

[17] A. van Hameren, C. G. Papadopoulos, and R. Pittau, Automated one-loop calculations: A proof of concept, J. High Energy Phys. 09 (2009) 106.

[18] A. van Hameren, OneLOop: For the evaluation of one-loop scalar functions, Comput. Phys. Commun. **182**, 2427 (2011).

[19] M. Czakon, C. G. Papadopoulos, and M. Worek, Polarizing the dipoles, J. High Energy Phys. 08 (2009) 085.

[20] G. Bevilacqua, M. Czakon, C. G. Papadopoulos, R. Pittau, and M. Worek, Assault on the NLO wishlist: $pp \to t\bar{t}b\bar{b}$, J. High Energy Phys. 09 (2009) 109.

[21] G. Bevilacqua, M. Czakon, M. Kubocz, and M. Worek, Complete Nagy-Soper subtraction for next-to-leading order calculations in QCD, J. High Energy Phys. 10 (2013) 204.

[22] J. Alwall *et al.*, A standard format for Les Houches event files, Comput. Phys. Commun. **176**, 300 (2007).

[23] I. Antcheva *et al.*, ROOT: A C++ framework for petabyte data storage, statistical analysis and visualization, Comput. Phys. Commun. **180**, 2499 (2009).

[24] Z. Bern, L. J. Dixon, F. Febres Cordero, S. Höche, H. Ita, D. A. Kosower, and D. Maitre, Ntuples for NLO events at hadron colliders, Comput. Phys. Commun. **185**, 1443 (2014).

[25] G. Bevilacqua (unpublished).

[26] P. Nason, A new method for combining NLO QCD with shower Monte Carlo algorithms, J. High Energy Phys. 11 (2004) 040,

[27] S. Frixione, P. Nason, and C. Oleari, Matching NLO QCD computations with parton shower simulations: The POWHEG method, J. High Energy Phys. 11 (2007) 070.

[28] S. Alioli, P. Nason, C. Oleari, and E. Re, A general framework for implementing NLO calculations in shower Monte Carlo programs: The POWHEG BOX, J. High Energy Phys. 06 (2010) 043.

[29] S. Frixione and B. R. Webber, Matching NLO QCD computations and parton shower simulations, J. High Energy Phys. 06 (2002) 029.

[30] C. Bierlich *et al.*, A comprehensive guide to the physics and usage of Pythia 8.3 SciPost Phys. Codebases **2022**, 8 (2022).

[31] A. Buckley, J. Butterworth, D. Grellscheid, H. Hoeth, L. Lonnblad, J. Monk, H. Schulz, and F. Siegert, Rivet user manual, Comput. Phys. Commun. **184**, 2803 (2013).
[32] C. Bierlich *et al.*, Robust independent validation of experiment and theory: Rivet version 3, SciPost Phys. **8**, 026 (2020).
[33] A. Buckley, P. Ilten, D. Konstantinov, L. Lönnblad, J. Monk, W. Pokorski, T. Przedzinski, and A. Verbytskyi, The HepMC3 event record library for Monte Carlo event generators, Comput. Phys. Commun. **260**, 107310 (2021).
[34] M. Cacciari and G. P. Salam, Dispelling the N^3 myth for the k_t jet-finder, Phys. Lett. B **641**, 57 (2006).
[35] M. Cacciari, G. P. Salam, and G. Soyez, FastJet user manual, Eur. Phys. J. C **72**, 1896 (2012).
[36] S. Frixione, S. Amoroso, and S. Mrenna, Matrix element corrections in the Pythia8 parton shower in the context of matched simulations at next-to-leading order, Eur. Phys. J. C **83**, 970 (2023).
[37] R. Frederix, L. Gellersen, and J. Nasufi, Matrix element corrections in top quark decays for the $t\bar{t}W^{\pm}$ process, Eur. Phys. J. C **84**, 410 (2024).
[38] P. Artoisenet, R. Frederix, O. Mattelaer, and R. Rietkerk, Automatic spin-entangled decays of heavy resonances in Monte Carlo simulations, J. High Energy Phys. 03 (2013) 015.
[39] S. Frixione, E. Laenen, P. Motylinski, and B. R. Webber, Angular correlations of lepton pairs from vector boson and top quark decays in Monte Carlo simulations, J. High Energy Phys. 04 (2007) 081.
[40] F. Febres Cordero, M. Kraus, and L. Reina, Top-quark pair production in association with a $W^{\pm}$ gauge boson in the Powheg-Box, Phys. Rev. D **103**, 094014 (2021).
[41] G. Bevilacqua, H.-Y. Bi, H. B. Hartanto, M. Kraus, M. Lupattelli, and M. Worek, $t\bar{t}b\bar{b}$ at the LHC: On the size of corrections and b-jet definitions, J. High Energy Phys. 08 (2021) 008.
[42] M. Czakon, A. Mitov, and R. Poncelet, Infrared-safe flavored anti-k_T jets, J. High Energy Phys. 04 (2023) 138.
[43] R. Gauld, A. Huss, and G. Stagnitto, Flavor identification of reconstructed hadronic jets, Phys. Rev. Lett. **130**, 161901 (2023); **132**, 159901(E) (2024).
[44] F. Caola, R. Grabarczyk, M. L. Hutt, G. P. Salam, L. Scyboz, and J. Thaler, Flavored jets with exact anti-kt kinematics and tests of infrared and collinear safety, Phys. Rev. D **108**, 094010 (2023).
[45] A. Behring *et al.*, flavored jet algorithms: A comparative study, J. High Energy Phys. 09 (2025) 149.
[46] R. D. Ball *et al.* (NNPDF Collaboration), Parton distributions from high-precision collider data, Eur. Phys. J. C **77**, 663 (2017).
[47] T.-J. Hou *et al.*, New CTEQ global analysis of quantum chromodynamics with high-precision data from the LHC, Phys. Rev. D **103**, 014013 (2021).